Atmospheric
Chemistry
and Physics
Discussions

Open Access

1 **Global streamflow and flood response to stratospheric aerosol geoengineering**

2 Liren Wei[1], Duoying Ji[1], Chiyuan Miao[2], John C. Moore[1,3,4]

3 [1]College of Global Change and Earth System Science, Beijing Normal University,
4 Beijing 100875, China
5 [2]State Key Laboratory of Earth Surface Processes and Resource Ecology, Faculty of
6 Geographical Science, Beijing Normal University, Beijing 100875, China
7 [3]Arctic Centre, University of Lapland, P.O. Box 122, 96101 Rovaniemi, Finland
8 [4]CAS Center for Excellence in Tibetan Plateau Earth Sciences, Beijing 100101, China

9

10 *Correspondence to:* Duoying Ji (duoyingji@gmail.com) or John C. Moore

11 (john.moore.bnu@gmail.com)

12 **Abstract:**

13 Flood risk is projected to increase under projections of future warming climates due to

14 an enhanced hydrological cycle. Solar geoengineering is known to reduce precipitation

15 and slowdown the hydrological cycle, and may be therefore be expected to offset

16 increased flood risk. We examine this hypothesis using streamflow and river discharge

17 responses to the representative concentration pathway RCP4.5 and Geoengineering

18 Model Intercomparison Project (GeoMIP) G4 experiments. We also calculate changes

19 in 30, 50, 100-year flood return periods relative to the historical (1960-1999) period

20 under the RCP4.5 and G4 scenarios. Similar spatial patterns are produced for each

21 return period, although those under G4 are closer to historical values than under RCP4.5.

22 Under G4 generally lower streamflows are produced on the western sides of Eurasia

23 and North America, with higher flows on their eastern sides. In the southern hemisphere

24 northern parts of the land masses have lower streamflow under G4, and southern parts

Atmospheric
Chemistry
and Physics
Discussions

Open Access

25   increases relative to RCP4.5. So in general solar geoengineering does appear to reduce

26   flood risk in most regions, but the relative effects are largely determined by this large

27   scale geographic pattern. Both streamflow and return period show increased drying of

28   the Amazon under both RCP4.5 and G4 scenarios, with more drying under G4.

29   **1. Introduction**

30   Floods cause considerable damage every year (UNISDR, 2013) that increases with

31   economic development and rate of climate change (Ward et al., 2017). Generally,

32   people and assets exposed to extreme hydrology disasters, including flooding, increase

33   under global warming (Alfieri et al., 2017; Arnell and Gosling, 2013; Tanoue et al.,

34   2016; Ward et al., 2013). Previous studies have shown that flood risk co-varies with

35   runoff and streamflow (Arnell and Gosling, 2013; Hirabayashi et al., 2013; Hirabayashi

36   et al., 2008). Hirabayashi et al. (2013) analyzed CMIP5 projections for the RCP4.5 and

37   RCP8.5 scenarios (Meinshausen et al., 2011), and found shortened return periods for

38   floods, especially in Southeast Asia, India and eastern Africa, especially under the

39   RCP8.5 scenario.

40

41   Koirala et al. (2014) analyzed the changes in streamflow conditions, that is high flow

42   (Q_5), low flow (Q_{95}) and mean flow (Q_m) under different RCP scenarios. Under the

43   RCP8.5 scenario, high flow increases at high latitudes, Asia and central Africa, while

44   mean and low flows decrease in Europe, western parts of North and central America.

45   Streamflow indicators under RCP4.5 show similar, but muted, spatial pattern as RCP8.5.

46

47   Other studies also show similar results with other hydrologic indicators and under other

48   future scenarios. For example, Arnell and Gosling, (2013) used a global scale daily

49   water balance hydrologic model (Mac-PDM.09; Gosling et al., 2010), forced by 21

50   climate CMIP3 models and analyzed 10-year and 100-year return period of maximum

51   daily flood under various scenarios. They found that the uncertainty in projecting river

52   streamflow is dominated by across-model differences rather than driven by the climate

53   scenario. Dankers et al. (2014) used 30-year return period of 5-day average peak flows

54   to study the changing patterns of flood hazard under the RCP8.5 scenario. They used

55   nine global hydrology models, together with five coupled climate models from CMIP5

56   and showed that simulated increases in flood risk occur in Siberia, Southeast Asia and

57   India, while decreases occur in northern and eastern Europe, and northwestern North

58   America. Flood frequency also decreased where the streamflow is dominated by spring

59   snow melt.

60

61   River flood models such as CaMa-Flood (Yamazaki et al., 2011) are important tools for

62   simulating flood hazard. These models have been combined with high resolution digital

63   elevation models, flow direction maps (e.g. HYDRO1k and HydroSHEDS; Lehner et

64   al., 2008), and hydrological models. The high-resolution models have contributed to

65   better simulation of river discharge (Yamazaki et al., 2009; Yamazaki et al., 2013 and

66   Mateo et al., 2017). Trigg et al., (2016) showed that six global river flood models

67   reproduced the flood patterns of large rivers satisfactorily. Inter-model variability in

Atmospheric
Chemistry
and Physics
Discussions

68   forcing from earth system models (ESM) are the major source of uncertainty in

69   modeling the river discharge (Vano et al., 2014; Winsemius, 2013; Mateo et al., 2017),

70   although the model ability to handle complex channels (e.g. deltas and floodplains) also

71   has an important impact on simulation realism.

72

73   Solar Radiation Management (SRM) is geoengineering designed to reduce the amount

74   of sunlight incident on the surface. Stratospheric aerosol injection is one SRM method

75   inspired by volcanic eruptions, that utilizes the aerosol direct effect to scatter incoming

76   solar radiation. Under the Geoengineering Model Intercomparison Project (GeoMIP;

77   Robock et al., 2011; Kravitz et al., 2011, 2012, 2013a), G4 experiment a constant 5Tg

78   per year of SO_2 is introduced into the lower tropical stratosphere of climate models

79   during the period of 2020-2069, while greenhouse gas forcing is defined by the RCP4.5

80   scenario. Indirect, potentially undesirable, side-effects of the injected sulfur aerosol

81   include changing ice particle distributions in the upper-troposphere, and the distribution

82   of ozone and water vapor in stratospheric (Visioni et al., 2017). The direct radiative

83   effects mainly result in the sharp reduction of TOA net radiative flux with a significant

84   drop in global surface temperature, and concomitant decrease in global precipitation

85   (Yu et al., 2015). The decline of precipitation under SRM is mainly due to increasing

86   atmospheric static stability, together with a reduction of latent heat flux from the land

87   surface to the atmosphere (Bala et al., 2008; Kravitz et al., 2013b; Tilmes et al., 2013).

88   Both the reduction of latent heat flux and precipitation result a slow-down of the global

89   hydrological cycle (Niemeier et al., 2013; Kalidindi et al., 2014; Ferraro and Griffiths,

Atmospheric
Chemistry
and Physics
Discussions

90   2016).

91

92   The spatial pattern of runoff roughly follows that of precipitation. Previous studies have

93   shown that under RCP4.5, precipitation would decrease over southern Africa, the

94   Amazon Basin and central America, and runoff follows these patterns. Over dry

95   continental interiors relatively large evaporation means that runoff does not follow

96   precipitation (Dai, 2016). SRM affects both precipitation and evaporation and hence

97   global patterns of runoff and thence streamflow. The risk of drought in dry regions

98   under SRM appears to be reduced (Curry et al., 2014; Keith and Irvine, 2016; Ji et al.

99   2018). While many studies have looked at the impact of geoengineering on the

100   hydrologic cycle, none has specifically considered the potential changes of river flow

101   and flood frequency.

102

103   We investigate the potential scenario of streamflow using annual mean and extreme

104   daily discharge, and changes in the pattern of flooding using flood return period.

105   Section 2 describes the models and methods used in this study; section 3 presents the

106   results of projected streamflow and return period under the G4 and RCP4.5 simulations.

107   Finally, section 4 provides a discussion of results and implications of this study.

108   **2. Data and Methods**

109   **2.1 GeoMIP experiments**

110   To analyze the potential changes of flood under stratospheric sulfate injection

Atmospheric
Chemistry
and Physics
Discussions

111   geoengineering, we compare the streamflow patterns under the RCP4.5 and G4

112   scenarios. Six models were used here (Table 1). We analyze the streamflow patterns

113   changes during the period 2030-2069 from each of model's G4 and RCP4.5 simulations.

114   The historical simulation during the period 1960-1999 is used as the reference for the

115   return period analysis. We used the same 40 years of G4 as Ji et al. (2018) used to

116   analyze extreme temperatures and precipitations.

117

118   In addition to the five ESM that provide the three simulation experiments in Table 1,

119   we utilize the GEOSCCM model that couples the Goddard Earth Observing System,

120   version 5 (GEO-5) (Rienecker et al., 2011) and a stratospheric chemistry module

121   (Pawson et al., 2008), but which has no historical simulation, and is only used for

122   streamflow simulations. The RCP4.5 and G4 experiments from GEOSCCM are forced

123   with sea surface temperature (SST) and sea ice concentrations simulated by the

124   Community Earth System Model (CESM; Gent et al., 2011). The single MIROC-ESM-

125   CHEM realization of the historical experiment is used as the reference in return period

126   calculations for all its realizations of the RCP4.5 and G4 experiments.

127

128   Table 1: GeoMIP models and experiments used in this study.

Model	Resolution (lon × lat, level)	Historical	RCP4.5	G4
BNU-ESM (Ji et al., 2014)	128 × 64, L26	1	1	1
CanESM2 (Arora et al., 2011; Chylek et al., 2011)	128 × 64, L35	3	3	3
GEOSCCM (Oman et al., 2011; Rienecker et al. 2008)	144 × 91, L72	×	3	3
MIROC-ESM (Watanabe et al., 2011)	128 × 64, L80	1	1	1
MIROC-ESM-CHEM (Watanabe et al., 2011)	128 × 64, L80	1	3	3
NorESM1-E (Bentsen et al. 2013, Tjiputra et al. 2013)	144 × 96, L26	1	1	1

129

2.2 The river routing model

130

131   The river routing model used here is the Catchment-based Macro-scale Floodplain

132   Model (CaMa-Flood; Yamazaki et al., 2011). The CaMa-Flood uses a local inertial flow

133   equation (Bates et al., 2010; Yamazaki et al., 2014a) to integrate runoff along a high-

134   resolution river map (HydroSHEDS; Yamazaki et al., 2013). Sub-grid characteristics

135   such as slope, river length, river channel width, river channel depth were parameterized

136   in each grid box by using the innovative up-scaling method, FLOW (Mateo et al., 2017;

137   Yamazaki et al., 2014b; Zhao et al., 2017). In addition, the CaMa-Flood implements

138   channel bifurcation and accounts for floodplain storage and backwater effects, which

139   are not represented in most global hydrological models (Zhao et al., 2017). CaMa-Flood

140   is able to reproduce relatively realistic flow patterns in complex river regions such as

141   deltas (Ikeuchi et al., 2015; Yamazaki et al., 2011, 2013) this makes it a well evaluated

142   model in hydrological research (Emerton et al., 2017; Ikeuchi et al., 2017; Suzuki et al.,

143   2017; Yamazaki et al., 2017; Zsótér et al., 2016).

144

145   We use only the daily runoff outputs from climate models to drive CaMa-Flood v3.6.2

146   which calculates the river discharge along the global river network. The spatial

147   resolution of CaMa-Flood was set to 0.25° (~25km at mid-latitude), and an adaptive

148   time step approach was applied in simulation. In order to conserve the input runoff mass,

149   an area-weighted averaging method was used in CaMa-Flood to distribute the coarse

150   input runoff to the fine resolution hydrological model. This down-scaling method is

151   available in the latest version of CaMa-Flood (Mateo et al., (2017). CaMa-Flood

Atmospheric
Chemistry
and Physics
Discussions

152   performs a 1-year spin-up before simulating 40-year river discharge in our historical,

153   RCP4.5 and G4 experiments. The runoff and river discharge from Antarctica and

154   Greenland are not included in CaMa-Flood simulations. For each streamflow level,

155   cells with less than 0.01 mm/day are excluded from the analysis.

2.3 Indicators of streamflow

157   We analyze the streamflow change under RCP4.5 and G4 scenarios using three

158   streamflow indicators during 2030-2069, that is annual daily mean flow (Q_m), and

159   extreme high or low flow (Q_5, Q_{95}: streamflow exceeded 5% or 95% of a year). Q_m, Q_5

160   and Q_{95} are averaged over 40 years for each model, respectively, then averaged between

161   models to get the multi-model mean response under different scenarios. We compared

162   the multi-model mean and multi-model median responses of the six models used in this

163   study, and found no obvious difference between the two averages.

164

165   We employ the two-sample Mann-Whitney U (MW-U) test to measure the significance

166   of streamflow differences between G4 and RCP4.5. The MW-U test is a non-parametric

167   test which does not need the assumption of normal probability distributions. We use a

168   bootstrap resampling method (Ward et al., 2016), with the MW-U test to increase

169   sample size and to minimize the effects of outliers that can arise from the relatively

170   short study period (Koirala et al., 2014). Specifically, we first apply the MW-U test to

171   the G4 and RCP4.5 raw annual mean daily runoff data for each model to get the value

172   of the rank sum statistical value, U_0. We generate 1000 random paired series of 40-

Atmospheric
Chemistry
and Physics
Discussions

173   year data from RCP4.5 and G4. Then the MW-U test was applied to each sample pair

174   of generated data to get a series of statistical values: U_j, $j = 1,2 \cdots 1000$. The rank of

175   U_0 is then used to calculate the non-exceedance probability (Cunnane, 1978):

176    $$p_0 = \frac{R_0 - 0.4}{N_b + 0.2}$$

177   Where p_0 is the non-exceedance probability and R_0 is the rank of U_0. N_b is the

178   number of the bootstrap samples. Finally, a non-exceedance probability less than 0.025

179   (or greater than 0.975) indicates a significant increase (or decrease) from RCP4.5 to G4,

180   respectively.

181   **2.4 Changes in flood frequency**

182   The return period of a flood event is as an indicator of flood frequency (e.g. Dankers et

183   al., 2014; Ward et al., 2017). The N-year return period indicates the probability of flood

184   exceeding a given level in any given year of 1/N. For each model, we choose the

185   historical period of 1960-1999 as a reference for the return period calculation based on

186   the annual maximum daily river discharge, then analyze the return period change under

187   RCP4.5 and G4 scenarios during the period of 2030-2069. In this study, we choose the

188   30, 50 and 100-year return period levels of river flow at each grid cell to study the

189   change of flood probability. To estimate the return period, the time series of annual

190   maximum daily discharge for historical, RCP4.5 and G4 from each ESM are first

191   arranged in ascending order and then fitted to a Gumbel probability distribution. The

192   Gumbel distribution was used as a statistic of extreme flood events in previous research

193   (e.g. Hirabayashi et al., 2013; Ward et al., 2014) Using the Gumbel distribution, the

Atmospheric
Chemistry
and Physics
Discussions

Open Access

194   cumulative distribution function, F(x), of river discharge (x) can be expressed as

195
$$F(x) = e^{-e^{-(\frac{x-b}{a})}}$$

196   where the two parameters a (scale) and b (location) are the parameters of Gumbel

197   distribution (Gumbel, 1941). The parameters are estimated using an L-moments based

198   approach (Rasmussen et al., 2003), where

199
$$L_1 = \frac{1}{N} \sum_{i=1}^{N} X_i$$

200
$$L_2 = \frac{2}{N} \sum_{i=1}^{N} \frac{i-1}{N-1} X_i - L_1$$

201   and X_i is the annual maximum daily river discharge and is sorted in ascending order

202   and N is the number of sample years, then:

203
$$a = \frac{L_2}{\ln 2}$$

204
$$b = L_1 - ac$$

205   where c = 0.57721 is Euler's constant. Changes in return period under geoengineering

206   are expressed as differences G4 - RCP4.5 relative to the corresponding historical level.

207   **3. Results**

208   **3.1 Projected changes in streamflow**

209   Figure 1 shows the relative changes of three characteristic indicators of streamflow,

210   while Figure 2 presents the degree of across-model agreement. Figures S1-S6 show the

211   results for each of the models listed in Table 1. In Fig. 1, positive values mean G4

212   streamflow is larger than RCP4.5 levels. Generally, decreases of the mean streamflow

213   (Q_m) occur at high northern latitudes such as Siberia, Northern Europe and the Arctic

Atmospheric
Chemistry
and Physics
Discussions

214   Ocean coast of North America, along with Southeast Asia, middle and southern Africa.

215   Increases appear in Western Europe, central Asia, southwestern North America and

216   central America (Fig. 1a). Significant changes are generally distributed around the

217   globe. Based on the ensemble response of the six models analyzed here, 57% of global

218   continental grid cells excluding Greenland, Antarctica and masked cells show decreases

219   in Q_m under G4 compared with RCP4.5, and about 43% of grid cells show increases.

220   Figure 2 showing areas with robust agreement between models allows the primary

221   regions affected to be seen more clearly. Globally, only 4.0% of grid cells exhibit robust

222   decreases and 4.4% increases under G4 (Fig. 2 a). Despite the few grid cells with robust

223   agreement between models, the general patterns are similar for the mean changes in Fig.

224   1a. Consistent decreases occur at high northern latitudes and in Papua New Guinea and

225   the semi-arid region south of the Sahara desert. Increases are mainly in the southern

226   hemisphere but also parts of Western Europe, and the southwestern USA. The

227   GEOSCCM (Fig. S3) and MIROC-ESM (Fig. S4) contradict the ensemble in having

228   larger areas with increases in Q_m under G4 than RCP4.5.

229

230   Figures 1b and 2b show that under G4, 55% of unmasked grid cells are projected to

231   increase their high flow Q_5 levels under G4. Europe, western North America, Central

232   Asia and central Australia show increases in Q_5 under G4 compared with RCP4.5.

233   Differences at the 95% significance level are distributed fairly similarly as for Q_m in

234   Figure 1a. The Amazon Basin shows decreases in both high flow and Q_m and the

235   southwestern USA shows increases in both. Globally, 4% of land cells show robust

Atmospheric
Chemistry
and Physics
Discussions

236   increases and 2% show decreases under G4 (Fig. 2b). Robust increases generally are

237   confined to the extra-tropics, while decreases are mainly, but not only, in the tropics.

238   The projections of Q_5 from CanESM2 under G4 show largest differences in spatial

239   pattern from the ensemble mean (Fig. S2) and it is the only model with more decreases

240   than increases in Q_5 under G4. Though high flow levels usually lead to flood events

241   (Ward et al., 2016), changes in flood levels do not necessarily translate into increases

242   in flood frequency. We elaborate further on flood return period in section 3.2.

243

244   Low flow (Q_{95}, in Figs. 1c and 2c) has a noisier spatial pattern than those for mean and

245   high flow. Low flow shows a relatively uniform decrease around the globe. 44% of

246   unmasked global land cells show increases in Q_{95} under G4. Despite the generally

247   noisier pattern, the regions with differences significant at the 95% level are more

248   defined for Q_{95} than either Q_m or Q_5. The high northern latitudes become drier under

249   G4, the southern high latitudes wetter. Robust increases cover about 2% of global land

250   grid cells, mainly in Europe and South America. Robust decreases appear mainly in

251   northern high-latitude regions, central Africa and northern Asia, and occupy about 6%

252   of global land grid cells. Projections by NorESM1-E (Fig. S6) and GEOSCCM (Fig.

253   S3) show different patterns from the ensemble mean (Fig. 1c) with bigger areas showing

254   increases than decreases in Q_{95} under G4.
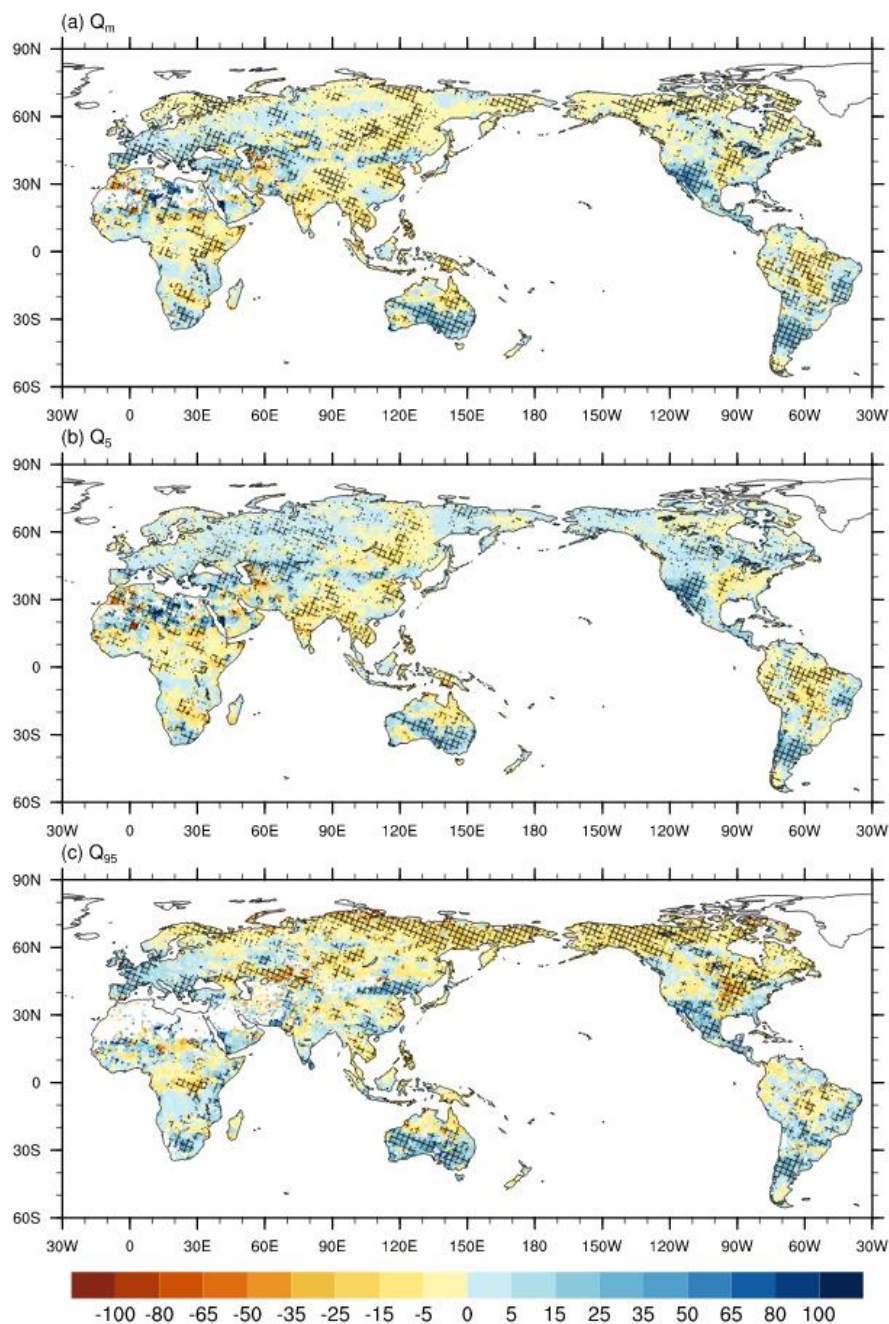
Figure 1: Relative difference of three streamflow indicators between G4 (2030-2069)
and RCP4.5 (2030-2069), as percentages of the mean of G4 and RCP4.5: $100\% \times$
$2(G4 - RCP4.5) / (G4 + RCP4.5)$. Top, long-term mean flow (Q_m); Middle, high flow
(Q_5); Bottom, low flow (Q_{95}). For each streamflow level, cells with less than 0.01

260   mm/day are masked out. Hashed areas indicate locations where the streamflow changes
261   are significant at the 95% level.

262
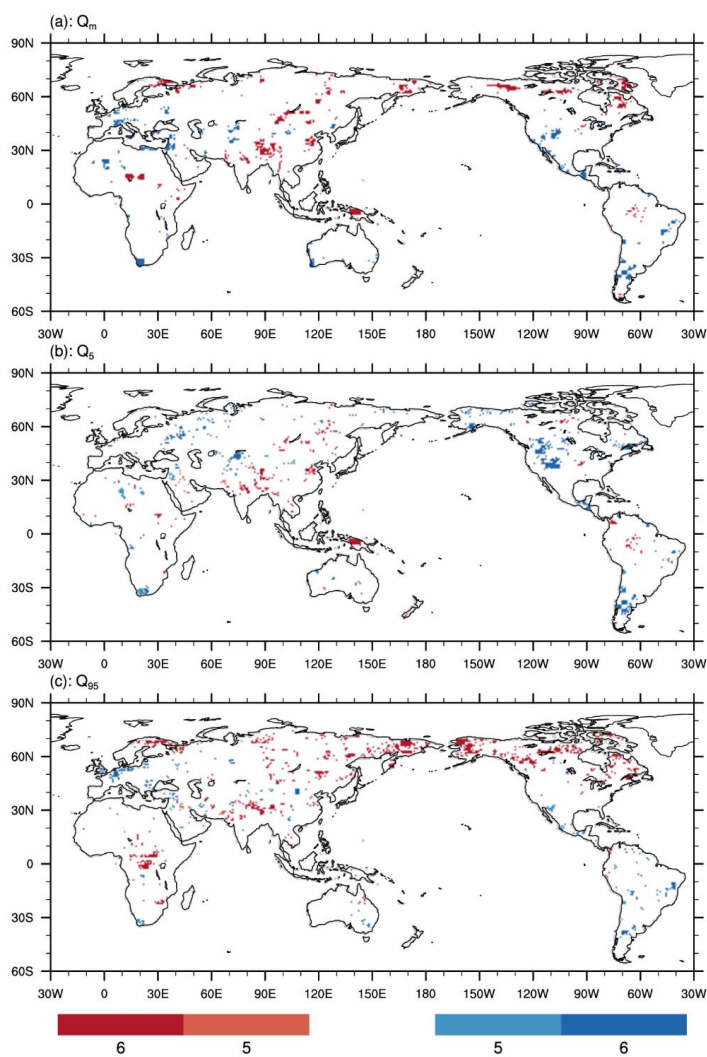
263

264   Figure 2: Number of model agreeing in sign (red means G4 - RCP4.5 <0, blue means
265   G4 - RCP4.5 >0) of streamflow indicator changes. Top, Q_m; Middle, Q_5; Bottom, Q_{95}.
266   Shaded grid cells indicate a relatively robust response (more than 4 models show same
267   change direction).

268

Atmospheric
Chemistry
and Physics
Discussions

269   Some of the regions show contrasting responses under G4 for high and low streamflow.

270   Figure 3 shows regions where both high and low flow decrease under G4 cover about

271   29% of grids cells, mainly in eastern and southeastern Asia, central Africa, and Amazon

272   Basin, together with central and eastern Siberia. In 16% of the cells high flows are

273   projected to increase while low flows decrease, mainly in the remaining parts of south

274   Asia, central Africa and South America. Increased high flow and simultaneous decrease

275   in low flow suggests the potential for increased flood and drought frequencies. In 27%

276   of global cells, high flows decrease and low flows increase, which suggests these would

277   see a decline in streamflow extremes, and are mainly at northern mid- and high-latitudes.

278   Areas with both increased high and low flow also cover 27% of the land surface, mainly

279   in Europe, central America and the southern hemisphere mid latitudes. Perhaps the

280   clearest overall pattern is the generally lower streamflow under G4 on the western sides

281   of the large continents of Eurasia and North America, with higher flows on their eastern

282   sides. In the southern hemisphere the pattern is meridional with northern parts of the

283   land masses having lower streamflow under G4, and southern parts increases.

284

Atmospheric
Chemistry
and Physics
Discussions
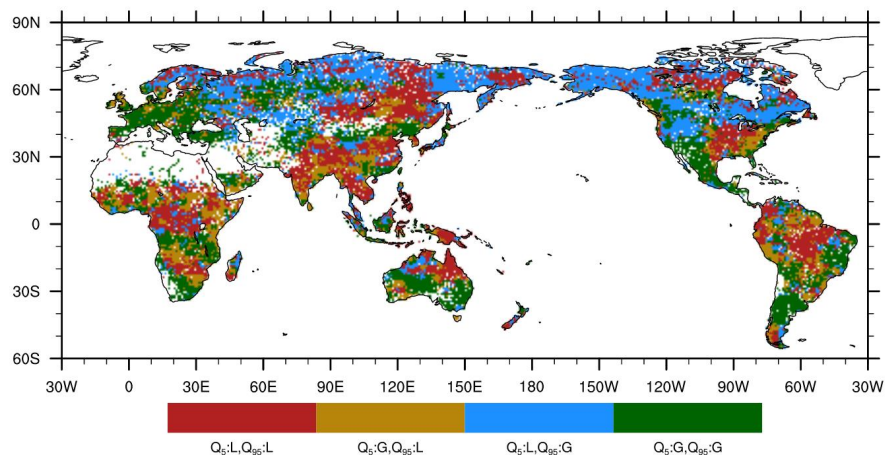
Figure 3: The ensemble mean differences (G4 - RCP4.5) of high and low streamflows. Color bar is defined such that grids where G4 is less than RCP4.5 for both Q5&Q95 is in red; Q5&Q95 greater in G4 than RCP4.5 is in green. Q5 greater in G4 and Q95 greater in RCP4.5 in yellow and vice versa in blue. Grid cells with Q_{95} less than 0.01 mm/day were masked.

3.2 Projected changes in return period

Changes in flooding between RCP4.5 and G4 scenarios are measured by the changes in the return period of particular river discharge magnitude. Previous studies have also used 30-year return period as a relatively modest indicator of flood frequency (Dankers et al., 2014). We choose both the same flooding frequency indicator and also the more extreme 50 or 100-year return levels. The discharge for each model's 30, 50 and 100-year return periods in the simulated historical period define the reference magnitudes at each grid cell. The return period of discharge corresponding to those levels are then found under the RCP4.5 and G4 scenarios. Dry regions, defined as mean annual streamflow during the historical period (1960-1999) less than 0.01 mm/day, are masked. The 40-year time series of the historical period (1960-1999) and 40-year future

303   projections (2030-2069) then are fitted to the Gumbel probability distribution for each

304   grid cell.

305

306   Figure 4a and 4b show the global distribution of multi-model ensemble median return

307   period of the historical 30-year return level, under the RCP4.5 and G4 scenarios. Figs.

308   S7 and S8 show the relevant patterns for 50 and 100-year return periods. The elongation

309   of return period in some regions (such as central Asia and the Amazon basin) indicates

310   relatively less frequent flooding events compared with the past. Very close to half the

311   grid cells (49%) show increases in return period under RCP4.5 scenario, while the other

312   half experience decreases. Increases of return period are mainly in Asia and eastern

313   Africa while decreases occur in Europe and North America. Our results agree with

314   similar previous studies (e.g., Hirabayashi et al., 2013) for RCP4.5. Under the

315   stratospheric aerosol injection G4 experiment the spatial pattern is very similar as

316   RCP4.5, with similar large differences from the historical levels.

317

318   Figure 4c shows the difference of return period between the G4 and RCP4.5 scenarios.

319   A negative value means a shorter return period under G4 than RCP4.5, which indicates

320   an increase of flood frequency under G4. Decreasing flood frequency appears in India,

321   China, Siberia, parts of the Amazon basin, and northern Australia. Increasing flood

322   frequencies are projected mainly in Europe, the southwestern USA and much of

323   Australia. The regions which are projected to experience an increased flood frequency

324   under the RCP4.5 scenario (Fig. 4a; Dankers et al., 2014; Hirabayashi et al., 2013)

325   would experience a consistent decline of the flood frequency under G4, such as

326   southern and southeastern Asia. In general, the G4 return periods are less changed from

327   the historical levels than under RCP4.5.

328

329   Figure 5 shows the regions of robust agreement between models in changes of 30-year

330   return period under RCP4.5 and G4. Slightly fewer grid cells show robust responses

331   under G4 than RCP4.5. As with Fig. 4 there is close agreement in spatial pattern of

332   return period under the RCP4.5 and G4 scenarios. The spatial pattern of the changes in

333   50 and 100-year return levels shown in Figs. S7 and S8 are similar to those for the 30-

334   year return level (Fig. 4), while the spread between two different return period levels is

335   slightly different from the 30-year levels. These results suggest a consistent changing

336   pattern of flood frequency as defined by the three return levels, but with different

337   magnitudes of differences between RCP4.5 and G4, with G4 being closer to the

338   historical levels.

339
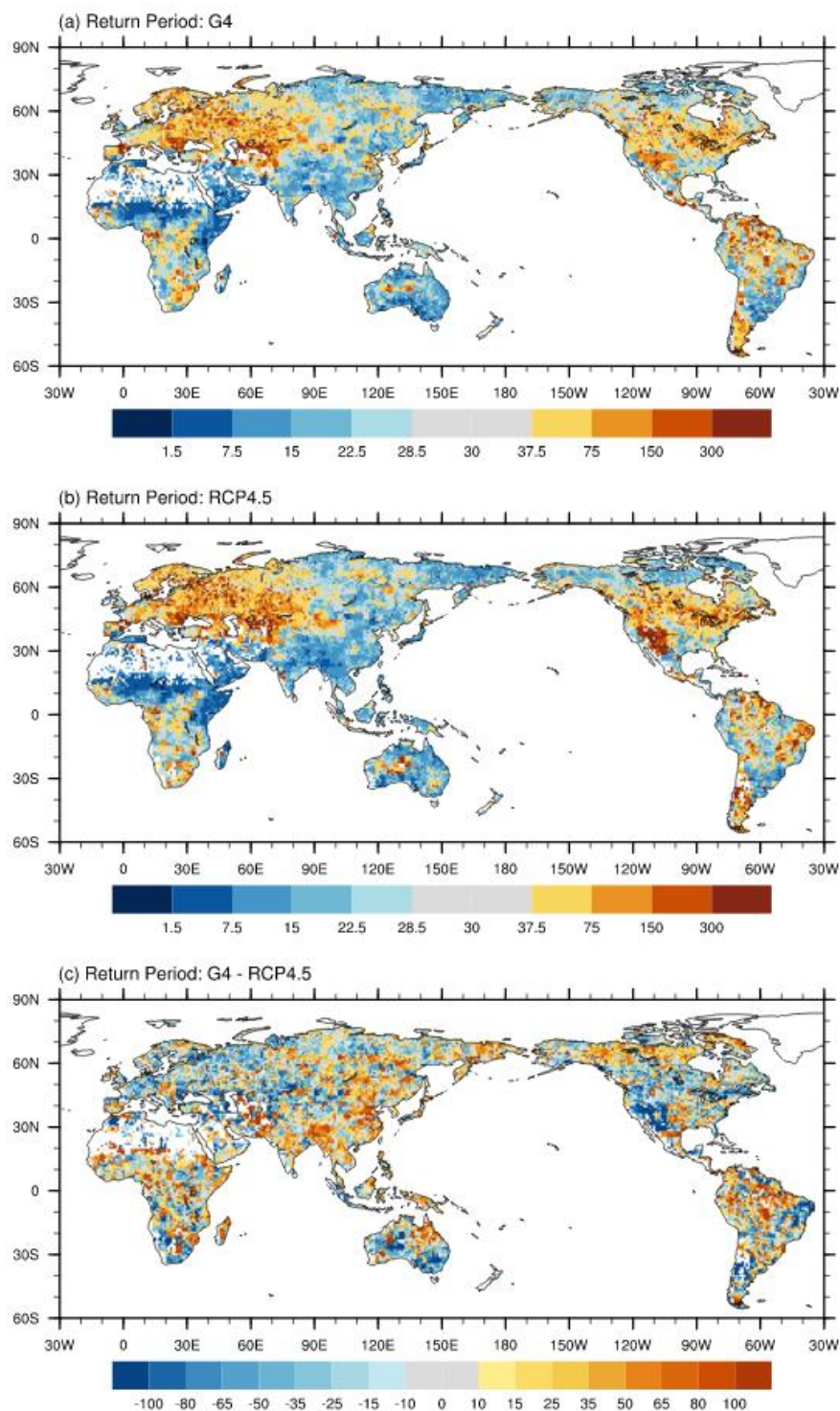
341   Figure 4: Multi-model ensemble median of return periods for discharge which correspond to 30-

342   year return period in the historical simulation (1960-1999) under (a) G4, (b) RCP4.5 scenarios and

343   (c) the relative difference of G4 and RCP4.5, as percentages of mean of return periods: $100\% \times$

344   $2(G4 - RCP4.5) / (G4 + RCP4.5)$. Grid cells in extremely dry regions, i.e. $Q_m < 0.01$ mm/day were

345   masked out.

346
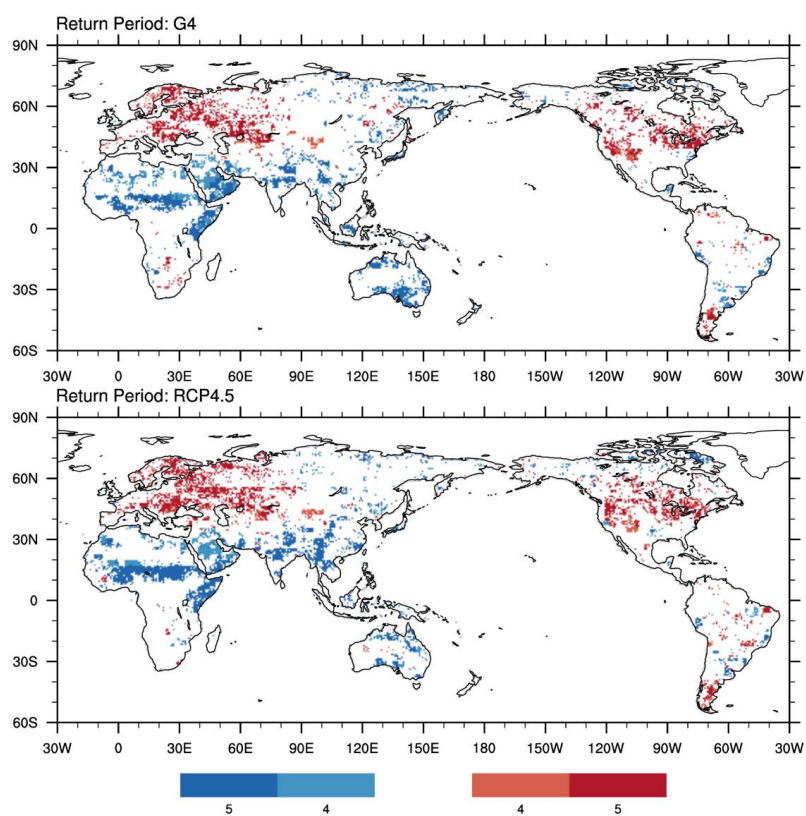
347

348   Figure 5: The number of models agreeing on the sign of change in 30-year return period under G4

349   (top panel) and RCP4.5 (bottom panel). Blue colors indicate decreases and red increases relative to

350   the historical simulation.

351

4. Discussion and Conclusions

353   We analyzed the streamflow response under the stratospheric aerosol injection

354   geoengineering, G4, and the RCP4.5 scenario using the daily total runoff from six

355   climate models that participated in GeoMIP. We investigated the mean change patterns

356   of mean and extreme high and low streamflow and analyzed the global flood frequency

357   change in terms of return period. There is pattern of generally lower streamflow under

358   G4 on the western sides of the large continents of Eurasia and North America, with

359   higher flows on their eastern sides. In the southern hemisphere the pattern is meridional

360   with northern parts of the land masses having lower streamflow under G4, and southern

361   parts increases.

362

363   These streamflow changes under G4 contrast with the pattern under RCP4.5 (Koirala

364   et al., 2014). For example, in southeastern Asia and India, both high flows and low

365   flows are projected to increase under the RCP4.5 scenario, while both of them would

366   decrease under G4. In contrast, Spain, Italy and Greece are projected to have decreases

367   in both high and low flow under RCP4.5, while the projected streamflow shows

368   increases under G4. However, in the Amazon basin, the streamflow decreases in both

369   high and low flow under both RCP4.5 and G4 relative to the historical period. In Siberia

370   both high and low streamflow increases under RCP4.5 relative to historical, while the

371   pattern is mixed under G4. This means that geoengineering offsets the impact

Atmospheric
Chemistry
and Physics
Discussions

Open Access

EGU

372   introduced by anthropogenic climate warming in some regions, while in other regions

373   such as the Amazon basin and Siberia, geoengineering further enhances the decreasing

374   trend of streamflow under the RCP4.5 scenario. The pattern seen is suggestive of the

375   role of large scale circulation patterns, westerly flows over the northern hemisphere

376   continents and the Asian monsoon systems, with relative increases in mid-latitude storm

377   systems and decreases in monsoons under G4 compared with RCP4.5; similar

378   mechanisms may also account for the north-south pattern seen in Australia and South

379   America. Monsoonal indicators do decrease under the much more extreme G1

380   experiment that is designed to offset quadrupled CO_2 levels (Tilmes et al., 2013).

381

382   We investigated the change of flooding corresponding to the magnitudes of the

383   historical 30, 50 and 100-year return period levels; the flooding frequencies change

384   dramatically from historical levels under both RCP4.5 and G4, but show similar spatial

385   patterns. The projected return period pattern under RCP4.5 scenario agrees well with

386   previous studies, such as Dankers et al., (2014) and Hirabayashi et al., (2013). Generally,

387   stratospheric aerosol injection geoengineering relieves flood stress especially for

388   Southeast Asia, and in turn increases the probability of flooding in the southwestern

389   USA and much of Australia – which are of course drought-prone places that might

390   benefit from increased flooding. The Amazon Basin shows a relatively elongation of

391   flood return period, while Europe shows shortening of return period under G4, and this

392   was also implicit in streamflow character in these regions.

393

394   Previous studies (Dankers et al., 2014; Hirabayashi et al., 2008) have noted that the

395   flood frequency for rivers at high latitude (e.g. Alaska and Siberia) decrease under

396   global warming even in areas where the frequency, intensity of precipitation, or both,

397   are projected to increase. The annual hydrograph of these rivers is dominated by snow

398   melt, so changes of peak flow reflect the balance between length and temperature of

399   winter season, and the total amount of winter precipitation. Under the G4 experiment,

400   some recent studies (Jones et al., 2018; Sonntag et al., 2018) have pointed out that the

401   increased P–E (difference between precipitation and evaporation) in northern Asia

402   caused by global warming could be partly counteracted by solar geoengineering. On

403   the other hand, compared with the RCP4.5 scenario, the SRM process reduces polar

404   temperatures (Berdahl et al., 2014). The balance among precipitation, evaporation and

405   temperature accounts for the complex spatial pattern of streamflow and flood frequency

406   at northern high-latitudes under G4, that has been previously been related to soil

407   moisture content (Dagon and Schrag, 2017).

408

409   The relatively dry pattern of streamflow in the Amazon basin under G4 is notable and

410   consistent with changes in P-E (e.g. Jones et al., 2018). This drying pattern would lead

411   to a decline of the Amazon tropical rainforest (Boisier et al., 2015). Amazon basin

412   drying is complicated by factors including the movement of Intertropical Convergence

413   Zone (ITCZ) under geoengineering (Smyth et al., 2017; Guo et al., 2018); changes in

414   SST reflecting changes in frequency of El Niño Southern Oscillation (Harris et al., 2008;

415   Jiménez-Muñoz et al., 2016), although there is no evidence of changes occurring under

Atmospheric
Chemistry
and Physics
Discussions

Open Access

EGU

416 SRM (Gabriel and Robock, 2015); and changes carbon cycle feedbacks (Chadwick et

417 al., 2017; Halladay and Good, 2017), which would certainly affected by changes in

418 diffuse radiation under SRM (Bala et al., 2008).

419

420 Limitations exist in our study. Model internal variability may be larger than across-

421 model spread in eastern and southeastern Asia (Yu et al., 2016). We assume that

422 systematic model bias relative to observations can be corrected by subtracting historical

423 simulations, and thus that model bias does not change with future climate scenario. We

424 ignore the effects of changing river routes and river network silt-up over time (Chezik

425 et al., 2017), which would impact local runoff and streamflow. The CaMa-Flood river

426 routing model also does not consider anthropogenic effects on rivers (e.g. dams), so the

427 results presented here are for a hypothetical natural condition.

428

429 Changes in flooding are strongly connected with the economic cost of damage due to

430 climate change and sea level rise (Jevrejva et al., 2016, Hinckel et al., 2014) and

431 thorough studies should be made for further policy and decision making, especially

432 applied to high value economic or ecological entities. This may be done in the

433 framework of specific impact models applied to local cities or regions, and would hence

434 benefit from local knowledge, especially in the developing world where resources for

435 adaptation measures are scarce. Linkages between the developing world climate

436 impacts researchers and the GeoMIP community will be encouraged and funded by the

437 DECIMALS project (Rahman et al., 2018).

Atmospheric
Chemistry
and Physics
Discussions

Open Access

EGU

References

Addor, N., Rössler, O., Köplin, N., Huss, M., Weingartner, R. and Seibert, J.: Robust changes and sources of uncertainty in the projected hydrological regimes of Swiss catchments, Water Resour. Res., 50(10), 7541–7562, doi:10.1002/2014WR015549, 2014.

Alfieri, L., Bisselink, B., Dottori, F., Naumann, G., de Roo, A., Salamon, P., Wyser, K. and Feyen, L.: Global projections of river flood risk in a warmer world, Earth's Futur., 5(2), 171–182, doi:10.1002/2016EF000485, 2017.

Arnell, N. W. and Gosling, S. N.: The impacts of climate change on river flow regimes at the global scale, J. Hydrol., 486, 351–364, doi:10.1016/j.jhydrol.2013.02.010, 2013.

Arora, V. K., Scinocca, J. F., Boer, G. J., Christian, J. R., Denman, K. L., Flato, G. M., Kharin, V. V, Lee, W. G. and Merryfield, W. J.: Carbon emission limits required to satisfy future representative concentration pathways of greenhouse gases, Geophys. Res. Lett., 38(5), 2011.

Bala, G., Duffy, P. B. and Taylor, K. E.: Impact of geoengineering schemes on the global hydrological cycle., Proc. Natl. Acad. Sci. U. S. A., 105(22), 7664–9,

Atmospheric
Chemistry
and Physics
Discussions

Open Access

EGU

461   doi:10.1073/pnas.0711648105, 2008.

462   Bates, P. D., Horritt, M. S. and Fewtrell, T. J.: A simple inertial formulation of the

463   shallow water equations for efficient two-dimensional flood inundation modelling, J.

464   Hydrol., 387(1–2), 33–45, doi:10.1016/j.jhydrol.2010.03.027, 2010.

465   Bentsen, M., Bethke, I., Debernard, J. B., Iversen, T., Kirkevåg, A., Seland, Ø., Drange,

466   H., Roelandt, C., Seierstad, I. A., Hoose, C. and Kristjánsson, J. E.: The Norwegian

467   Earth System Model, NorESM1-M – Part 1: Description and basic evaluation of the

468   physical climate, Geosci. Model Dev., 6(3), 687–720, doi:10.5194/gmd-6-687-2013,

469   2013.

470   Berdahl, M., Robock, A., Ji, D., Moore, J. C., Jones, A., Kravitz, B. and Watanabe, S.:

471   Arctic cryosphere response in the Geoengineering Model Intercomparison Project G3

472   and   G4   scenarios,   J.   Geophys.   Res.   Atmos.,   119(3),   1308–1321,

473   doi:10.1002/2013JD020627, 2014.

474   Boisier, J. P., Ciais, P., Ducharne, A. and Guimberteau, M.: Projected strengthening of

475   Amazonian dry season by constrained climate model simulations, Nat. Clim. Chang.,

476   5(7), 656–660, doi:10.1038/nclimate2658, 2015.

477   Chadwick, R., Douville, H. and Skinner, C. B.: Timeslice experiments for

478   understanding regional climate projections: applications to the tropical hydrological

479   cycle   and   European   winter   circulation,   Clim.   Dyn.,   49(9–10),   3011–3029,

480   doi:10.1007/s00382-016-3488-6, 2017.

481   Chezik, K. A., Anderson, S. C. and Moore, J. W.: River networks dampen long-term

482   hydrological   signals   of   climate   change,   Geophys.   Res.   Lett.,

483   doi:10.1002/2017GL074376, 2017.

484   Chylek, P., Li, J., Dubey, M. K., Wang, M. and Lesins, G.: Observed and model

485   simulated 20th century Arctic temperature variability: Canadian Earth System Model

486   CanESM2, Atmos. Chem. Phys. Discuss., 11(8), 22893–22907, doi:10.5194/acpd-11-

487   22893-2011, 2011.

488   Clark, M. P., Wilby, R. L., Gutmann, E. D., Vano, J. A., Gangopadhyay, S., Wood, A.

489   W., Fowler, H. J., Prudhomme, C., Arnold, J. R. and Brekke, L. D.: Characterizing

490   Uncertainty of the Hydrologic Impacts of Climate Change, Curr. Clim. Chang. Reports,

491   2(2), 55–64, doi:10.1007/s40641-016-0034-x, 2016.

492   Cunnane, C.: Unbiased Plotting Position - A Review, J. Hydrol., 37(3), 205–222, 1978.

493   Curry, C. L., Sillmann, J., Bronaugh, D., Alterskjaer, K., Cole, J. N. S., Ji, D., Kravitz,

494   B., Kristjánsson, J. E., Moore, J. C., Muri, H., Niemeier, U., Robock, A., Tilmes, S. and

495   Yang, S.: A multimodel examination of climate extremes in an idealized geoengineering

496   experiment, J. Geophys. Res. G Biogeosciences, 119(7), 3900–3923,

497   doi:10.1002/2013JD020648, 2014.

498   Dai, A.: Historical and Future Changes in Streamflow and Continental Runoff: A

499   Review, Terr. Water Cycle Clim. Chang. Nat. Human-Induced Impacts, 17–37,

500   doi:10.1002/9781118971772.ch2, 2016.

501   Dagon, K. and Schrag, D. P.: Regional Climate Variability Under Model Simulations

502   of Solar Geoengineering, J. Geophys. Res. Atmos., 1–16, doi:10.1002/2017JD027110,

503   2017.

504   Dankers, R., Arnell, N. W., Clark, D. B., Falloon, P. D., Fekete, B. M., Gosling, S. N.,

Atmospheric
Chemistry
and Physics
Discussions
Open Access

505   Heinke, J., Kim, H., Masaki, Y., Satoh, Y., Stacke, T., Wada, Y. and Wisser, D.: First

506   look at changes in flood hazard in the Inter-Sectoral Impact Model Intercomparison

507   Project   ensemble,   Proc.   Natl.   Acad.   Sci.,   111(9),   3257–3261,

508   doi:10.1073/pnas.1302078110, 2014.

509   Ehsani, N., Vörösmarty, C. J., Fekete, B. M. and Stakhiv, E. Z.: Reservoir Operations

510   Under Climate Change: Storage Capacity Options to Mitigate Risk, J. Hydrol., 555,

511   435–446, doi:10.1016/j.jhydrol.2017.09.008, 2017.

512   Emerton, R., Cloke, H. L., Stephens, E. M., Zsoter, E., Woolnough, S. J. and

513   Pappenberger, F.: Complex picture for likelihood of ENSO-driven flood hazard, Nat.

514   Commun., 8, 14796, doi:10.1038/ncomms14796, 2017.

515   Ferraro, A. J. and Griffiths, H. G.: Quantifying the temperature-independent effect of

516   stratospheric aerosol geoengineering on global-mean precipitation in a multi-model

517   ensemble, Environ. Res. Lett., 11(3), 34012, doi:10.1088/1748-9326/11/3/034012,

518   2016.

519   Gabriel, C. J. and Robock, A.: Stratospheric geoengineering impacts on El

520   Niño/Southern Oscillation, Atmos. Chem. Phys., 15(6), 9173–9202, 2015.

521   Gent, P. R., Danabasoglu, G., Donner, L. J., Holland, M. M., Hunke, E. C., Jayne, S. R.,

522   Lawrence, D. M., Neale, R. B., Rasch, P. J., Vertenstein, M., Worley, P. H., Yang, Z. L.

523   and Zhang, M.: The community climate system model version 4, J. Clim., 24(19),

524   4973–4991, doi:10.1175/2011JCLI4083.1, 2011.

525   Gosling, S. N., Bretherton, D., Haines, K. and Arnell, N. W.: Global hydrology

526   modelling and uncertainty: running multiple ensembles with a campus grid, Philos.

527   Trans. R. Soc. A Math. Phys. Eng. Sci., 368(1926), 4005–4021,

528   doi:10.1098/rsta.2010.0164, 2010.

529   Gumbel, E. J.: The Return Period of Flood Flows, Ann. Math. Stat., 12(2), 163–190,

530   doi:10.1214/aoms/1177731747, 1941.

531   Halladay, K. and Good, P.: Non-linear interactions between CO_2 radiative and

532   physiological effects on Amazonian evapotranspiration in an Earth system model, Clim.

533   Dyn., 49(7–8), 2471–2490, doi:10.1007/s00382-016-3449-0, 2017.

534   Harris, P. P., Huntingford, C. and Cox, P. M.: Amazon Basin climate under global

535   warming: the role of the sea surface temperature, Philos. Trans. R. Soc. B Biol. Sci.,

536   363(1498), 1753–1759, doi:10.1098/rstb.2007.0037, 2008.

537   Hattermann, F. F., Krysanova, V., Gosling, S. N., Dankers, R., Daggupati, P., Donnelly,

538   C., Flörke, M., Huang, S., Motovilov, Y., Buda, S., Yang, T., Müller, C., Leng, G., Tang,

539   Q., Portmann, F. T., Hagemann, S., Gerten, D., Wada, Y., Masaki, Y., Alemayehu, T.,

540   Satoh, Y. and Samaniego, L.: Cross-scale intercomparison of climate change impacts

541   simulated by regional and global hydrological models in eleven large river basins, Clim.

542   Change, 141(3), 561–576, doi:10.1007/s10584-016-1829-4, 2017.

543   Haywood, J. M., Jones, A., Bellouin, N. and Stephenson, D.: Asymmetric forcing from

544   stratospheric aerosols impacts Sahelian rainfall, Nat. Clim. Chang., 3(7), 660–665,

545   doi:10.1038/nclimate1857, 2013.

546   Hirabayashi, Y., Kanae, S., Emori, S., Oki, T. and Kimoto, M.: Global projections of

547   changing risks of floods and droughts in a changing climate, Hydrol. Sci. J., 53(4), 754–

548   772, doi:10.1623/hysj.53.4.754, 2008.

549   Hirabayashi, Y., Mahendran, R., Koirala, S., Konoshima, L., Yamazaki, D., Watanabe,

550   S., Kim, H. and Kanae, S.: Global flood risk under climate change, Nat. Clim. Chang.,

551   3(9), 816–821, doi:10.1038/nclimate1911, 2013.

552   Hinkel, J., Lincke, D., Vafeidis, A. T., Perrette, M., Nicholls, R. J., Tol, R. S. J.,

553   Marzeion, B., Fettweis, X., Ionescu, C. and Levermannet, A.: Coastal flood damage

554   and adaptation costs under 21st century sea-level rise, Proc. Natl. Acad. Sci. USA, 111,

555   3292–3297, 2014.

556   Ikeuchi, H., Hirabayashi, Y., Yamazaki, D., Kiguchi, M., Koirala, S., Nagano, T., Kotera,

557   A. and Kanae, S.: Modeling complex flow dynamics of fluvial floods exacerbated by

558   sea level rise in the Ganges–Brahmaputra–Meghna Delta, Environ. Res. Lett., 10(12),

559   124011, doi:10.1088/1748-9326/10/12/124011, 2015.

560   Ikeuchi, H., Hirabayashi, Y., Yamazaki, D., Muis, S., Ward, P. J., Winsemius, H. C.,

561   Verlaan, M. and Kanae, S.: Compound simulation of fluvial floods and storm surges in

562   a global coupled river-coast flood model: Model development and its application to

563   2007 Cyclone Sidr in Bangladesh, J. Adv. Model. Earth Syst., 9(4), 1847–1862,

564   doi:10.1002/2017MS000943, 2017.

565   Jevrejeva, S., Jackson, L. P., Riva, R. E. M., Grinsted, A. and Moore, J. C.: Coastal sea

566   level rise with warming above 2°C, Proc. Natl Acad. Sci. USA, 113, 13342–13347,

567   2016.

568   Ji, D., Wang, L., Feng, J., Wu, Q., Cheng, H., Zhang, Q., Yang, J., Dong, W., Dai, Y.,

569   Gong, D., Zhang, R. H., Wang, X., Liu, J., Moore, J. C., Chen, D. and Zhou, M.:

570   Description and basic evaluation of Beijing Normal University Earth System Model

571   (BNU-ESM) version 1, Geosci. Model Dev., 7(5), 2039–2064, doi:10.5194/gmd-7-

572   2039-2014, 2014.

573   Ji, D., Fang, S., Curry, C. L., Kashimura, H., Watanabe, S., Cole, J. N. S., Lenton, A.,

574   Muri, H., Kravitz, B., and Moore, J. C.: Extreme temperature and precipitation response

575   to solar dimming and stratospheric aerosol geoengineering, Atmos. Chem. Phys.

576   Discuss., https://doi.org/10.5194/acp-2018-131, in review, 2018.

577   Jiménez-Muñoz, J. C., Mattar, C., Barichivich, J., Santamaría-Artigas, A., Takahashi,

578   K., Malhi, Y., Sobrino, J. A. and Schrier, G. Van Der: Record-breaking warming and

579   extreme drought in the Amazon rainforest during the course of El Niño 2015-2016, Sci.

580   Rep., 6(September), 1–7, doi:10.1038/srep33130, 2016.

581   Jones, A. C., Hawcroft, M. K., Haywood, J. M., Jones, A., Guo, X. and Moore, J. C.:

582   Regional climate impacts of stabilizing global warming at 1.5 K using solar

583   geoengineering, Earth's Futur., 1–22, doi:10.1002/2017EF000720, 2018.

584   Kalidindi, S., Bala, G., Modak, A. and Caldeira, K.: Modeling of solar radiation

585   management: a comparison of simulations using reduced solar constant and

586   stratospheric sulphate aerosols, Clim. Dyn., 44(9–10), 2909–2925,

587   doi:10.1007/s00382-014-2240-3, 2014.

588   Keith, D. W. and Irvine, P. J.: Solar geoengineering could substantially reduce climate

589   risks—A research hypothesis for the next decade, Earth's Futur., 4(11), 549–559,

590   doi:10.1002/2016EF000465, 2016.

591   Koirala, S., Hirabayashi, Y., Mahendran, R. and Kanae, S.: Global assessment of

592   agreement among streamflow projections using CMIP5 model outputs, Environ. Res.

593   Lett., 9(6), 64017, doi:10.1088/1748-9326/9/6/064017, 2014.

594   Kravitz, B., Robock, A., Boucher, O., Schmidt, H., Taylor, K. E., Stenchikov, G. and

595   Schulz, M.: The Geoengineering Model Intercomparison Project (GeoMIP), Atmos. Sci.

596   Lett., 12(2), 162–167, doi:10.1002/asl.316, 2011.

597   Kravitz, B., Robock, A. and Haywood, J. M.: Progress in climate model simulations of

598   geoengineering, Eos (Washington. DC)., 93(35), 340, doi:10.1029/2012EO350009,

599   2012.

600   Kravitz, B., Robock, A., Forster, P. M., Haywood, J. M., Lawrence, M. G. and Schmidt,

601   H.: An overview of the Geoengineering Model Intercomparison Project (GeoMIP), J.

602   Geophys. Res. Atmos., 118(23), 13103–13107, doi:10.1002/2013JD020569, 2013a.

603   Kravitz, B., Caldeira, K., Boucher, O., Robock, A., Rasch, P. J., Alterskjær, K., Karam,

604   D. B., Cole, J. N. S., Curry, C. L., Haywood, J. M., Irvine, P. J., Ji, D., Jones, A.,

605   Kristjánsson, J. E., Lunt, D. J., Moore, J. C., Niemeier, U., Schmidt, H., Schulz, M.,

606   Singh, B., Tilmes, S., Watanabe, S., Yang, S. and Yoon, J. H.: Climate model response

607   from the Geoengineering Model Intercomparison Project (GeoMIP), J. Geophys. Res.

608   Atmos., 118(15), 8320–8332, doi:10.1002/jgrd.50646, 2013b.

609   Lehner, B., Verdin, K. and Jarvis, K.: New global hydrograghy derived from spaceborne

610   elevation data, Eos, Trans. AGU, 89(10), 93–94, doi:10.1029/2008EO100001, 2008.

611   Mateo, C. M. R., Yamazaki, D., Kim, H., Champathong, A., Vaze, J. and Oki, T.:

612   Impacts of spatial resolution and representation of flow connectivity on large-scale

613   simulation of floods, Hydrol. Earth Syst. Sci., 21(10), 5143–5163, doi:10.5194/hess-

614   21-5143-2017, 2017.

Atmospheric
Chemistry
and Physics
Discussions

Open Access

EGU

615   Meinshausen, M., Smith, S. J., Calvin, K., Daniel, J. S., Kainuma, M. L. T., Lamarque,

616   J-F., Matsumoto, K., Montzka, S. A., Raper, S. C. B., Riahi, K., Thomson, A., Velders,

617   G. J. M., van Vuuren, D. P. P.: The RCP greenhouse gas concentrations and their

618   extensions from 1765 to 2300, Climatic Change, 109:213, doi:10.1007/s10584-011-

619   0156-z, 2011.

620   Niemeier, U., Schmidt, H., Alterskjær, K. and Kristjánsson, J. E.: Solar irradiance

621   reduction via climate engineering: Impact of different techniques on the energy balance

622   and the hydrological cycle, J. Geophys. Res. Atmos., 118(21), 11905–11917,

623   doi:10.1002/2013JD020445, 2013.

624   Niemeier, U. and Tilmes, S.: Sulfur injections for a cooler planet, Science (80-.).,

625   357(6348), 246–248, doi:10.1126/science.aan3317, 2017.

626   Oman, L. D., Ziemke, J. R., Douglass, A. R., Waugh, D. W., Lang, C., Rodriguez, J. M.

627   and Nielsen, J. E.: The response of tropical tropospheric ozone to ENSO, Geophys. Res.

628   Lett., 38(13), 2–7, doi:10.1029/2011GL047865, 2011.

629   Pawson, S., Stolarski, R. S., Douglass, A. R., Newman, P. A., Nielsen, J. E., Frith, S.

630   M. and Gupta, M. L.: Goddard earth observing system chemistry-climate model

631   simulations of stratospheric ozone-temperature coupling between 1950 and 2005, J.

632   Geophys. Res. Atmos., 113(12), 1–16, doi:10.1029/2007JD009511, 2008.

633   Pitari, G., Aquila, V., Kravitz, B., Robock, A., Watanabe, S., Cionni, I., Luca, N. De,

634   Genova, G. Di, Mancini, E. and Tilmes, S.: Stratospheric ozone response to sulfate

635   geoengineering: Results from the Geoengineering Model Intercomparison Project

636   (GeoMIP), J. Geophys. Res. Atmos., 119(5), 2629–2653, doi:10.1002/2013JD020566,

637   2014.

638   Rahman, A., Artaxo, P., Asrat, A., and Parker, A.: Developing countries must lead on

639   solar geoengineering research, Nature, in press.

640   Rasmussen, P. F. and Gautam, N.: Alternative PWM-estimators of the gumbel

641   distribution, J. Hydrol., 280(1–4), 265–271, doi:10.1016/S0022-1694(03)00241-5,

642   2003.

643   Rienecker, M. M. and Coauthors: The GEOS-5 Data Assimilation System—

644   Documentation of versions 5.0.1 and 5.1.0, and 5.2.0, NASA Tech. Rep. Ser. Glob.

645   Model. Data Assim. NASA/TM-2008-104606, 27(December), 92pp,

646   doi:10.2759/32049, 2008.

647   Rienecker, M. M., Suarez, M. J., Gelaro, R., Todling, R., Bacmeister, J., Liu, E.,

648   Bosilovich, M. G., Schubert, S. D., Takacs, L. and Kim, G.-K.: MERRA: NASA's

649   modern-era retrospective analysis for research and applications, J. Clim., 24(14), 3624–

650   3648, 2011.

651   Robock, A., Kravitz, B. and Boucher, O.: Standardizing experiments in geoengineering,

652   in Eos, vol. 92, p. 197., 2011.

653   Sonntag, S., Ferrer González, M., Ilyina, T., Kracher, D., Nabel, J. E. M. S., Niemeier,

654   U., Pongratz, J., Reick, C. H. and Schmidt, H.: Quantifying and Comparing Effects of

655   Climate   Engineering   Methods   on   the   Earth   System,   Earth's   Futur.,

656   doi:10.1002/2017EF000620, 2018.

657   Suzuki, T., Yamazaki, D., Tsujino, H., Komuro, Y., Nakano, H. and Urakawa, S.: A

658   dataset of continental river discharge based on JRA-55 for use in a global ocean

Atmospheric
Chemistry
and Physics
Discussions

659   circulation model, J. Oceanogr., (123456789), doi:10.1007/s10872-017-0458-5, 2017.

660   Tanoue, M., Hirabayashi, Y. and Ikeuchi, H.: Global-scale river flood vulnerability in

661   the last 50 years, Sci. Rep., 6(1), 36021, doi:10.1038/srep36021, 2016.

662   Tilmes, S., Fasullo, J., Lamarque, J. F., Marsh, D. R., Mills, M., Alterskjær, K., Muri,

663   H., Kristjánsson, J. E., Boucher, O., Schulz, M., Cole, J. N. S., Curry, C. L., Jones, A.,

664   Haywood, J., Irvine, P. J., Ji, D., Moore, J. C., Karam, D. B., Kravitz, B., Rasch, P. J.,

665   Singh, B., Yoon, J. H., Niemeier, U., Schmidt, H., Robock, A., Yang, S. and Watanabe,

666   S.: The hydrological impact of geoengineering in the Geoengineering Model

667   Intercomparison Project (GeoMIP), J. Geophys. Res. Atmos., 118(19), 11036–11058,

668   doi:10.1002/jgrd.50868, 2013.

669   Tjiputra, J. F., Roelandt, C., Bentsen, M., Lawrence, D. M., Lorentzen, T., Schwinger,

670   J., Seland and Heinze, C.: Evaluation of the carbon cycle components in the Norwegian

671   Earth System Model (NorESM), Geosci. Model Dev., 6(2), 301–325, doi:10.5194/gmd-

672   6-301-2013, 2013.

673   Trigg, M. A., Birch, C. E., Neal, J. C., Bates, P. D., Smith, A., Sampson, C. C., Yamazaki,

674   D., Hirabayashi, Y., Pappenberger, F., Dutra, E., Ward, P. J., Winsemius, H. C., Salamon,

675   P., Dottori, F., Rudari, R., Kappes, M. S., Simpson, A. L., Hadzilacos, G. and Fewtrell,

676   T. J.: The credibility challenge for global fluvial flood risk analysis, Environ. Res. Lett.,

677   11(9), 94014, doi:10.1088/1748-9326/11/9/094014, 2016.

678   UNISDR (The United Nations International Strategy for Disaster Reduction): Global

679   Assessment Report on Disaster Risk Reduction: From Shared Risk to Shared Value –

680   The Business Case for Disaster Risk Reduction, Glob. Assess. Rep. Disaster Risk

681   Reduct., 246, 2013.

682   Vano, J. A., Udall, B., Cayan, D. R., Overpeck, J. T., Brekke, L. D., Das, T., Hartmann,

683   H. C., Hidalgo, H. G., Hoerling, M., McCabe, G. J., Morino, K., Webb, R. S., Werner,

684   K. and Lettenmaier, D. P.: Understanding uncertainties in future Colorado River

685   streamflow, Bull. Am. Meteorol. Soc., 95(1), 59–78, doi:10.1175/BAMS-D-12-

686   00228.1, 2014.

687   Visioni, D., Pitari, G. and Aquila, V.: Sulfate geoengineering: A review of the factors

688   controlling the needed injection of sulfur dioxide, Atmos. Chem. Phys., 17(6), 3879–

689   3889, doi:10.5194/acp-17-3879-2017, 2017.

690   Wada, Y., de Graaf, I. E. M. and van Beek, L. P. H.: High-resolution modeling of human

691   and climate impacts on global water resources, J. Adv. Model. Earth Syst., 8(2), 735–

692   763, doi:10.1002/2015MS000618, 2016.

693   Ward, P. J., Jongman, B., Weiland, F. S., Bouwman, A., van Beek, R., Bierkens, M. F.

694   P., Ligtvoet, W. and Winsemius, H. C.: Assessing flood risk at the global scale: model

695   setup, results, and sensitivity, Environ. Res. Lett., 8(4), 44019, doi:10.1088/1748-

696   9326/8/4/044019, 2013.

697   Ward, P. J., Kummu, M. and Lall, U.: Flood frequencies and durations and their

698   response to El Niño Southern Oscillation: Global analysis, J. Hydrol., 539, 358–378,

699   doi:10.1016/j.jhydrol.2016.05.045, 2016.

700   Ward, P. J., Jongman, B., Aerts, J. C. J. H., Bates, P. D., Botzen, W. J. W., DIaz Loaiza,

701   A., Hallegatte, S., Kind, J. M., Kwadijk, J., Scussolini, P. and Winsemius, H. C.: A

702   global framework for future costs and benefits of river-flood protection in urban areas,

703   Nat. Clim. Chang., 7(9), 642–646, doi:10.1038/nclimate3350, 2017.

704   Watanabe, S., Hajima, T., Sudo, K., Nagashima, T., Takemura, T., Okajima, H., Nozawa,

705   T., Kawase, H., Abe, M., Yokohata, T., Ise, T., Sato, H., Kato, E., Takata, K., Emori, S.

706   and Kawamiya, M.: MIROC-ESM 2010: Model description and basic results of

707   CMIP5-20c3m experiments, Geosci. Model Dev., 4(4), 845–872, doi:10.5194/gmd-4-

708   845-2011, 2011.

709   Winsemius, H. C., Van Beek, L. P. H., Jongman, B., Ward, P. J. and Bouwman, A.: A

710   framework for global river flood risk assessments, Hydrol. Earth Syst. Sci., 17(5),

711   1871–1892, doi:10.5194/hess-17-1871-2013, 2013.

712   Yamazaki, D., Oki, T. and Kanae, S.: Deriving a global river network map and its sub-

713   grid topographic characteristics from a fine-resolution flow direction map, Hydrol.

714   Earth Syst. Sci., 13(11), 2241–2251, doi:10.5194/hess-13-2241-2009, 2009.

715   Yamazaki, D., Kanae, S., Kim, H. and Oki, T.: A physically based description of

716   floodplain inundation dynamics in a global river routing model, Water Resour. Res.,

717   47(4), 1–21, doi:10.1029/2010WR009726, 2011.

718   Yamazaki, D., De Almeida, G. A. M. and Bates, P. D.: Improving computational

719   efficiency in global river models by implementing the local inertial flow equation and

720   a vector-based river network map, Water Resour. Res., 49(11), 7221–7235,

721   doi:10.1002/wrcr.20552, 2013.

722   Yamazaki, D., O'Loughlin, F., Trigg, M. A., Miller, Z. F., Pavelsky, T. M. and Bates, P.

723   D.: Development of the Global Width Database for Large Rivers, Water Resour. Res.,

724   50(4), 3467–3480, doi:10.1002/2013WR014664, 2014a.

Atmospheric
Chemistry
and Physics
Discussions

725   Yamazaki, D., Sato, T., Kanae, S., Hirabayashi, Y. and Bates, P. D.: Regional flood

726   dynamics in a bifurcating mega delta simulated in a global river model, Geophys. Res.

727   Lett., 41(9), 3127–3135, doi:10.1002/2014GL059744, 2014b.

728   Yamazaki, D., Ikeshima, D., Tawatari, R., Yamaguchi, T., O'Loughlin, F., Neal, J. C.,

729   Sampson, C. C., Kanae, S. and Bates, P. D.: A high-accuracy map of global terrain

730   elevations, Geophys. Res. Lett., 44(11), 5844–5853, doi:10.1002/2017GL072874, 2017.

731   Yu, M., Wang, G. and Chen, H.: Quantifying the impacts of land surface schemes and

732   dynamic vegetation on the model dependency of projected changes in surface energy

733   and   water   budgets,   J.   Adv.   Model.   Earth   Syst.,   8(1),   370–386,

734   doi:10.1002/2015MS000492, 2016.

735   Zhao, F., Veldkamp, T. I. E., Frieler, K., Schewe, J., Ostberg, S., Willner, S.,

736   Schauberger, B., Gosling, S. N., Schmied, H. M., Portmann, F. T., Leng, G., Huang, M.,

737   Liu, X., Tang, Q., Hanasaki, N., Biemans, H., Gerten, D., Satoh, Y., Pokhrel, Y., Stacke,

738   T., Ciais, P., Chang, J., Ducharne, A., Guimberteau, M., Wada, Y., Kim, H. and

739   Yamazaki, D.: The critical role of the routing scheme in simulating peak river discharge

740   in global hydrological models, Environ. Res. Lett., 12(7), 75003, doi:10.1088/1748-

741   9326/aa7250, 2017.

742   Zsótér, E., Pappenberger, F., Smith, P., Emerton, R. E., Dutra, E., Wetterhall, F.,

743   Richardson, D., Bogner, K. and Balsamo, G.: Building a Multimodel Flood Prediction

744   System   with   the   TIGGE   Archive,   J.   Hydrometeorol.,   17(11),   2923–2940,

745   doi:10.1175/JHM-D-15-0130.1, 2016.